



MoC_x species embedded in ordered mesoporous silica framework with hierarchical structure for hydrogenation of naphthalene



Min Pang^a, Xiaozhen Chen^a, Qinying Xu^b, Changhai Liang^{a,*}

^a Laboratory of Advanced Materials & Catalytic Engineering, Dalian University of Technology, Dalian 116024, PR China

^b Science and Technology on Surface Physics and Chemistry Laboratory, P.O. Box 718-35, Mianyang 621700, PR China

ARTICLE INFO

Article history:

Received 26 May 2014

Received in revised form

13 November 2014

Accepted 17 November 2014

Available online 22 November 2014

Keywords:

Molybdenum carbide

Incorporation

Single-source precursor

Naphthalene hydrogenation

Tetralin

ABSTRACT

An integrated route to accomplish the incorporation of MoC_x species into ordered mesoporous silica framework (OMSF) was presented. The Mo^{VI}-melamine hybrids were used as the single-source precursors for molybdenum carbides and participated in the assembling process of the silica building blocks that gave rise to the OMSF preform. The pore diameter and the volume of the resulting MoC_x@OMSF samples were characterized by gradually increasing with the amount of the added hybrids, which, among other things, maximized the space inside the silica tubes at the highest Mo loading. The thermal decomposition of the P123 micelles with the catalysis of the in situ formed Mo species generated the tube-like carbon framework within the silica tubes. The finely incorporation of the MoC_x species to the carbon framework was supposed to account for the good stability of the carbide phase in the hydrogenation of naphthalene. Ultra-high selectivity of ~98% to tetralin was achieved on the MoC_x@OMSF samples thanks to the moderate hydrogenating ability of the carbide phase, indicating potential use of molybdenum carbide based composites as low-cost selective catalysts for industrially relevant partial hydrogenations.

© 2014 Elsevier B.V. All rights reserved.

1. Introduction

Molybdenum carbides, ever since the disclosure of their Pt-like catalytic behaviors [1], have drawn ever-growing interest in the context of them being the partial replacement or ultimate alternative to precious metal catalysts [2–5]. In fact, it is quite often to observe them display inspiring performances in a variety of lab-scale reactions ranging from hydrogenation to isomerization [6–10]. However, in industrial scale, deactivation is one big issue due to which molybdenum carbides are not yet widely applied. Surface carbon deposit inherited from the preparation and thermal sintering of the particles during reaction are two main open questions to be addressed concerning the applicability of molybdenum carbides in long-term practical use. To tackle these problems, molybdenum carbides have to be prepared with single phase and, in the mean time, immobilized by suitable supports. Separately speaking, synthetic methods involving external carbon sources, frequently used such as hydrocarbons, solid carbon, and CO_x, for carburization are unable to generate a clean carbide surface owing to a gradient of carbon toward the particle core [11]. Thus in order to reduce the carbon concentration and the consequent huge

risk of coke formation in the surface region of the particles, the carbon diffusion has to be inverted. To this end, the state-of-art methodology to obtain single phase molybdenum carbides via the so-called single-source precursor route. The key to this technique is coordinating the carbon sources with Mo sources through chemical bonds forming a new molecule, namely the single-source precursor. Herein, introducing external carbon sources for carburization in the sequent thermal treatment becomes unnecessary. Furthermore, all the redox reactions contained in this route are temperature-induced and confined within the precursor, which means the in situ formed carbon-containing gas products such as CO, CO₂, or CH₄ are going to escape the particle body via an outward diffusion. Thus when the carbon-containing gases diffuse from the bulk to the gas-solid interface along the content-descending direction, they are further diluted and taken away by carrier gas (e.g. Ar, He) instead of accumulating there to form surface carbon contaminants. Typical single-source precursors, for instance Mo^{VI}-hexamethylenetetramine hybrids [12], Mo^{VI}-aniline hybrids [13], and Mo^{VI}-melamine hybrids revealed and studied in depth by our group [14], have demonstrated their applicability to synthesize single phase molybdenum carbide by simple thermal treatment.

In another aspect, single phase molybdenum carbide suffers from low surface area (typically below 100 m²/g) thus has to be combined with supports to improve the dispersion as well as the resistance to thermal sintering. Generally, there is an impregnating

* Corresponding author. Tel.: +86 411 84986353; fax: +86 411 84986353.

E-mail address: changhai@dlut.edu.cn (C. Liang).

of the Mo precursors with the supports, followed by calcination and carburization [15,16]. The dispersion of the resultant carbides on the supports is therefore determined by the impregnation procedure. Unfortunately, most of the results were unsatisfactory, exhibiting carbides either locally aggregating or unincorporated into the framework of the supports. These carbide particles are thermally unstable thanks to the weak contact with the supports that under certain harsh reaction conditions they would undergo thermal sintering, leading to activity loss and shortening of the service life. Advanced methods have been delivered to enhance the coalescence between the carbides and the supports in order to improve the carbides durability in catalytic use. In this regard, Ji et al. had taken advantage of Mo species interplaying with P123 micelles in the fabrication of SBA-15 to achieve the inclusion of MoO_x into the silica framework. Followed by CH_4 -carburization, the highly dispersive MoO_x were transformed into $\beta\text{-Mo}_2\text{C}$ which preserved the intimate connection of that between MoO_x and the support, featuring good thermal stability [17]. Zhang et al. had introduced an organic–organic cooperative self-assembly approach to imbed MoC nanoparticles (NPs) into the ordered mesoporous carbon. The resorcinol resin, which was used as the bridge agent in the synthesis, first assembled around F127 micelles then interacted with $\text{Mo}_7\text{O}_{24}^{6-}$ groups. After the carburization of MoO_x by the resin, MoC NPs were evenly decorated into the carbon walls derived from the pyrolysis of the resin, and strongly anchored to the carbon support [18]. The two examples just demonstrated how to achieve the target of finely distributing carbides within the framework of the supports in a self-assembly manner. Yet, the key question remains, while there is either a way to obtain molybdenum carbides with single phase by eliminating the use of external carbon sources, or a way to incorporate them into the framework of the supports by the operation of self-assembly but still preserving the carburization of MoO_x by free unbonded carbon, there is a blank of the integration of the two techniques; and those composites with single phase carbide finely included in the support framework remains a good solution to the aforementioned two deactivation issues of molybdenum carbides catalysts but still a big challenge.

The key objective of our research has been to combine those two routes together in one way. To accomplish this goal, we applied the Mo^{VI} –melamine hybrids reported in our earlier work as the single-source precursors for single phase molybdenum carbides. The hybrids were arranged with the building blocks for mesoporous silica in a designate order through the self-assembly effect to form the $\text{MoC}_x@\text{OMSF}$ preform. Followed by a simple thermal treating procedure without introducing external carbon sources, the preform was turned into the final composite with MoC_x species evenly embedded in the ordered mesoporous silica framework (OMSF).

2. Experimental

2.1. Catalysts preparation

Poly(ethylene oxide)–Poly(propylene oxide)–Poly(ethylene oxide) (Aldrich, pluronic, P-123). Ammonium heptamolybdate (AHM), melamine (MA), and tetraethyl orthosilicate (TEOS) were purchased from Sinopharm Chemical Reagent Co., Ltd. All the reagents were used as achieved without further purification.

The Mo^{VI} –melamine hybrids ($\text{Mo}_{19}\text{O}_{66}(\text{C}_3\text{H}_7\text{N}_6)_{18}\cdot 12\text{H}_2\text{O}$) were synthesized following the procedure reported in the previous literature [14]. In a typical synthesis, the hybrids were obtained by mixing the aqueous solutions of AHM and MA, and collecting the white precipitate. Heating H_2O to 80 °C was necessary to completely dissolve MA. The aqueous solution of MA was allowed to cool to RT naturally because either a dramatic decline of temperature or any mechanical disturbance would induce the precipitation of MA from water.

For the synthesis of MoC_x incorporated into ordered mesoporous silica framework of SBA type with varied Si/Mo molar ratios, 2 g of P123 was dissolved in 50 mL HCl (2.5 M). The temperature of the solution was kept at 40 °C using a water bath. A certain amount of the hybrids was added into the P123 solution. Exceptionally, due to the limited amount of the hybrids dissolved in HCl at 40 °C, the hybrids were first dissolved in 50 mL HCl (2.5 M) at 80 °C in synthesizing the sample with Si/Mo molar ratio equaling 6. The solution was then used to dissolve P123 after being cooled to 40 °C. After stirring at 40 °C for 5 h, 5.82 g of TEOS was added in, and soon later, the solution became opaque indicating the hydrolysis of TEOS. After stirring at 40 °C for another 5 h, the opaque system was transferred into a 100 mL Teflon autoclave and isothermally treated at 100 °C for 24 h. The precipitate was collected by filtration but without washing and, dried at 120 °C. Pyrolyzing the precipitate in Ar/H_2 (100 mL/min, 1:1 (v/v)) led to $\text{MoC}_x@\text{OMSF}$ samples with varied Si/Mo molar ratios. The temperature was increased linearly from RT to 650 °C with a linear increase of 5 °C/min and hold at 650 °C for 90 min. The gas was switched off after the temperature dropped to 300 °C below to allow the slow diffusion of air back into the quartz tube to passivate the carbide surface in order to avoid bulk oxidation. The as-prepared samples were denoted as $\text{MoC}_x@\text{OMSF-70, 50, 30, 15, 10, 6}$, where the number corresponded to the Si/Mo molar ratio. Pure OMSF was prepared for comparison. Its synthesis was identical to that for the $\text{MoC}_x@\text{OMSF}$ sample but without the addition of the Mo^{VI} –melamine hybrids. The reference sample free of silica was prepared according to the preparation procedure for the $\text{MoC}_x@\text{OMSF}$ samples but without adding TEOS. After the Mo^{VI} –melamine hybrids were dissolved in the solution of P123, the mixture was transferred into a 100 mL Teflon autoclave and isothermally treated at 100 °C for 24 h. The solvent was removed through rotary evaporation at 60 °C. The collected gel was dried in oven at 120 °C before subjected to thermal treatment identical to that in the preparation of the $\text{MoC}_x@\text{OMSF}$ samples.

The $\text{Mo}@\text{OMSF}$ sample was prepared through the wet impregnation method. Pure OMSF was impregnated in the aqueous solution of AHM for 12 h. The collected powder was subjected to thermal treatment in Ar/H_2 (100 mL/min, 2:3 (v/v)) after dried in oven at 120 °C. The temperature was increased linearly from RT to 700 °C with a linear increase of 5 °C/min and hold at 700 °C for 240 min.

Bulk $\beta\text{-Mo}_2\text{C}$ was obtained by directly pyrolyzing the Mo^{VI} –melamine hybrids in Ar/H_2 (100 mL/min, 1:1 (v/v)). The temperature was increased linearly from RT to 650 °C with a linear increase of 5 °C/min and hold at 650 °C for 90 min [14].

2.2. Catalyst characterizations

X-ray diffraction measurements were taken on a Rigaku D/MAX 2400 diffractometer with $\text{Cu K}\alpha$ radiation. Nitrogen adsorption–desorption isotherms were measured at 77 K by using ASiQC0000-4 (Quantachrome Instrument Co.). Samples were degassed in a vacuum at 200 °C for 12 h. The total pore volumes were estimated from the adsorbed amount of N_2 at a relative pressure P/P_0 of 0.95. CHN elemental analysis was performed on an Elementar Vario EL system. Fourier transform infrared (FT-IR) spectra were collected at room temperature on a Nicolet Impact 410 spectrometer with a resolution of 4 cm^{-1} . Raman spectra were recorded on a DXR Raman Microscope with excitation line at 532 nm. The molar ratios of Si to Mo were determined by inductively coupled plasma-atomic emission spectroscopy (ICP-AES) after the samples were dissolved in 10 M NaOH. Field-emission scanning electron microscopic (FE-SEM) observations were achieved by using a NOVA NanoSEM 450 system. Dynamic light scattering (DLS) measurements were made on a ZETASIZER nano series Nano-ZS90 (Malvern Instrument Co.) and zeta potentials were determined using the same instrument with

a zeta potential analyzer. Transmission electron microscopy (TEM) was performed using a Philips CM200 FEG transmission electron microscope equipped with energy-dispersive X-ray spectroscopy (EDX). X-Ray photoelectron spectroscopy (XPS) measurements were carried out in an ultra-high vacuum (UHV) set-up equipped with a Gammadata-Scienta SES 2002 analyzer and used the main C 1s peak at 284.5 eV as reference.

2.3. Catalytic activity test

The hydrogenation of naphthalene was carried out in a cylindrical fixed-bed stainless steel reactor (12 mm × 2 mm × 500 mm). A certain amount of the catalyst was diluted with quartz sand and loaded in the thermostatic section of the reactor. The rest part of the reactor was filled with quartz sand. Then the reactor was heated to 400 °C at a rate of 10 °C/min under 0.5 MPa H₂ and kept for 1.5 h to get the catalyst refreshed. After the reactor was cooled to 340 °C, a desired amount of cyclohexane with 1 wt.% naphthalene was introduced into the reactor under 4 MPa H₂ at a given flow rate. The steady state was achieved after reacting for 12 h. The amounts of tetralin and decalin were determined by an Agilent 7890-II gas chromatograph equipped with an OV-101 capillary column (5 m) and a FID detector.

3. Results and discussion

3.1. Formation mechanism

Fig. 1 illustrated the formation process of the MoC_x@OMSF. The self-assembly of P123 in HCl formed hexagonal-packed cylindrical micelles, which were positively charged due to the surface ethylene oxide groups. The P123 micelles then accommodated the Mo^{VI}-melamine hybrids by complexing the MoO_x species with the surface ethylene oxides, as demonstrated by the color of the solution changing into yellow upon the addition of the hybrids [19]. Further adding TEOS, the hydrolysis of –Si–O–CH₂–CH₃ into –Si–OH happened in attachment to the hybrids bonded with the P123 micelles, forming the MoC_x@OMSF preform. Since the Mo^{VI}-melamine hybrids were proved to be single-source precursors for molybdenum carbides, the following pyrolysis of the preform gave rise to MoC_x species in situ formed within the silica tubes. The assembling process was further proved by DLS measurements. The hydrodynamic radius (R_H) of the P123 micelles was observed to increase with the amount of the added hybrids, as the attached hybrids which possessed a molecular weight of 5382 with big volume [14] effectively expanded the volume of the P123 micelles (**Fig. 2a**). In correspondence with the increasing amount of the attached hybrids was the decrease of the surface electronic

potential of the P123 micelles, as the positive charge from the ethylene oxides was neutralized by the negative charge from the MoO_x species within the hybrids (**Fig. 2b**).

3.2. Structural characterization

The N₂ physisorption isotherms of the MoC_x@OMSF samples exhibited the typical type IV features with H1 hysteresis loops, characteristic of an ordered mesoporous structure (**Fig. 3a**). A well-defined, sharp inflection at $P/P_0 = 0.6\text{--}0.8$ was observed in the adsorption branches of the isotherms, indicating a narrow pore size distribution within the mesopore range (**Fig. 3b**). The detailed results of N₂ physisorption were summarized in **Table 1**. A marked increase of 0.8 nm in the pore diameter of the sample was observed upon the inclusion of the hybrids. Further adding the hybrids resulted in a gradual increase of the pore diameter and the total pore volume of the MoC_x@OMSF samples. The pore diameter of the sample reached the maximum of 7.5 nm when the Mo/Si molar ratio increased to 1/10. Further increasing the Mo/Si molar ratio to 1/6 did not bring obvious changes, which was explained by the saturation of the accommodation capability of the P123 micelles for the hybrids. In contrast to the conventional wet impregnation method, in which the increase of the metal species lead to the gradual decrease of the pore diameter and the volume of the resulting sample, the presented preparation procedure by use of the expanding effect of the hybrids on the volume of the template micelles for silica tubes maximized the space inside the silica tubes at the highest Mo loading.

Small-angle X-ray diffraction patterns of the samples presented three typical diffraction peaks indexed to (1 0 0), (1 1 0), and (2 0 0) reflections in the hexagonal space group p6mm, characteristic of a SBA-type architecture [20] (**Fig. 4b**). The latter two reflections were intensified upon the involvement of MoC_x, probably due to the introduction of salts can enhance the long-range order of the silica framework [21]. The three peaks were well resolved irrespective of the Mo loading, indicating the inclusion of MoC_x did not bring periodicity loss or induce phase transformation. Apart from the three peaks, an additional diffraction peak emerged in the 2θ range of 1–1.5°, which was supposed to be an indication for the formation of the tube-like carbon framework within the silica tubes. The average I_G/I_D value derived from the Raman spectra demonstrated the high graphitization degree of the carbon residues within the MoC_x@OMSF samples while also implied that the Mo species formed somewhere during the pyrolysis catalyzed the graphitization of carbon, as the carbon residues in pure OMSF were amorphous (**Fig. 4a**). The TG-DTA curves indicated that the Mo species in situ formed during the pyrolysis of the MoC_x@OMSF preform remarkably affected the thermal decomposition of the P123

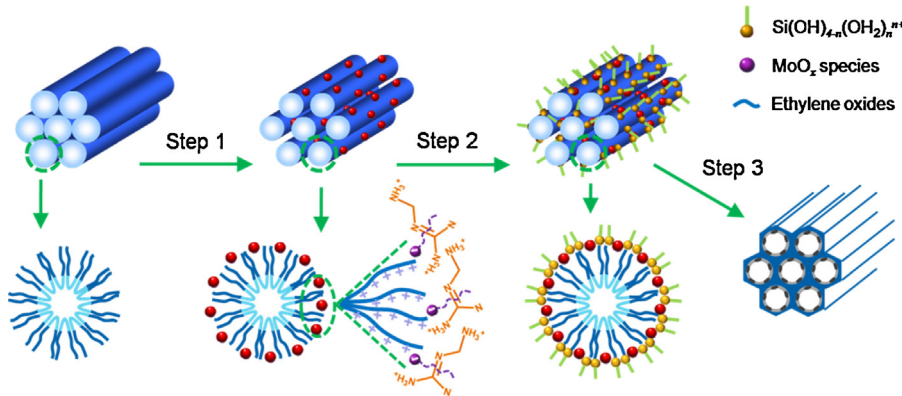


Fig. 1. Illustration of the formation process for the MoC_x@OMSF composite.

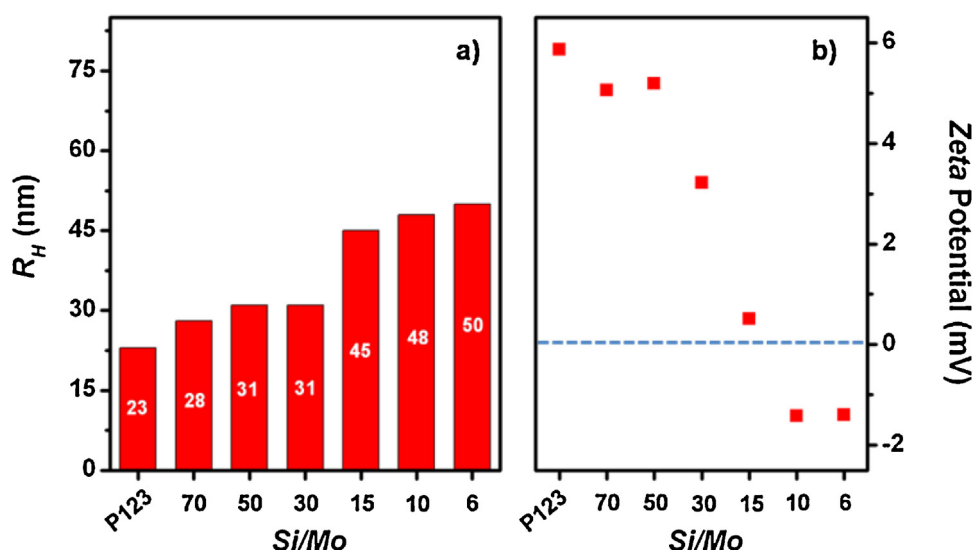


Fig. 2. Hydrodynamic radius (a) and zeta potential (b) of the surfactant micelles in dependence of Si/Mo molar ratio.

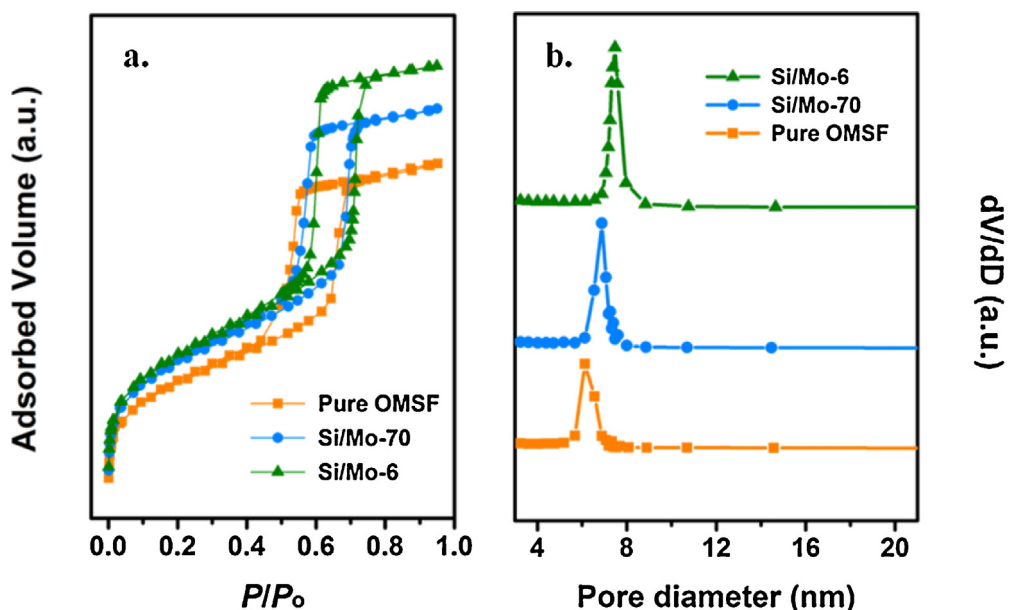


Fig. 3. N_2 adsorption–desorption isotherms (a) and pore size distribution (b) of the $\text{MoC}_x@\text{OMSF}$ samples derived from the adsorption branches.

Table 1

Textural properties of the $\text{MoC}_x@\text{OMSF}$ samples.

Si/Mo	Mo (wt.%)	C (wt.%)	$S_{\text{BET}}^{\text{a}}$ ($\text{m}^2 \text{g}^{-1}$)	$S_{\text{BET}}^{\text{b}}$ ($\text{m}^2 \text{g}^{-1}$)	$D_{\text{BJH}}^{\text{c}}$ (nm)	V_p^{d} ($\text{cm}^3 \text{g}^{-1}$)	V_p^{e} ($\text{cm}^3 \text{g}^{-1}$)	$V_{\text{micro}}^{\text{f}}$ (%)	W^{g} (nm)
∞	0	0.21	646	646	6.1	0.76	0.76	0.12	1.6
70	0.3	0.88	739	741	6.9	0.88	0.88	0.12	2.3
50	0.4	0.93	829	833	7.3	0.99	0.99	0.13	2.3
30	0.9	1.07	809	816	7.2	0.99	1.00	0.11	2.3
15	1.6	1.33	798	811	7.3	1.00	1.02	0.10	2.3
10	1.7	1.37	787	800	7.5	1.00	1.01	0.11	2.7
6	2.7	1.41	771	793	7.5	0.97	1.00	0.11	2.8
6 ^h	ND ⁱ	— ^j	806	—	7.6	1.02	1.43	0.11	—

^a Determined by BET method.

^b Normalized $S_{\text{BET}} = S_{\text{BET}} / (1 - \text{content}_{[\text{Mo}]})$.

^c Determined by BJH method.

^d Total pore volume at $P/P_0 = 0.95$.

^e Normalized $V_p = V_p / (1 - \text{content}_{[\text{Mo}]})$.

^f Calculated by t-plot method.

^g Wall thickness of carbon tubes = $(d_{100} - d_{100})/\sqrt{3}/2$.

^h $\text{MoC}_x@\text{OMSF}-6$ after thermal treating in O_2 at 550°C for 6 h.

ⁱ Not determined.

^j Cannot be detected with certainty.

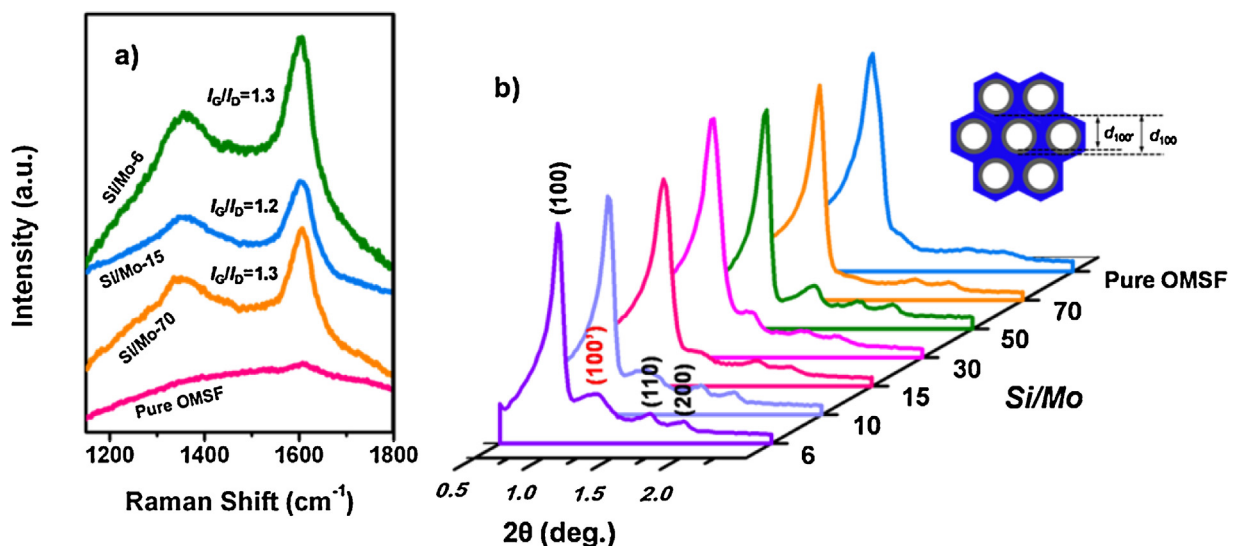


Fig. 4. Raman spectra (a) and small-angle XRD patterns (b) of the $\text{MoC}_x@\text{OMSF}$ samples. Inset in (b) was the illustration for the $(100')$ reflection.

micelles, which process posed larger weight loss and ended at lower temperature with the participation of the Mo^{VI} –melamine hybrids from the very beginning (Fig. S1). Hence, the tube-like carbon framework was supposed to result from the thermal decomposition of the P123 micelles with the catalysis of the in situ formed Mo species. The decomposition process gave rise to graphitic flakes, some of which bordered each other somewhere along the silica tube to form the tube-like structure. The melamine within the hybrids also contributed to the graphitic flakes, as the N 1s XPS spectrum indicated the N residues (~0.03 wt.%) were mainly in form of pyridine-N, pyrrole-N, and oxidized N (Fig. S2). The newly emerged peak in the XRD pattern could be indexed to the $(100')$ reflection arising from the interference by the inner walls of the silica tubes and the “carbon tubes”. The wall thickness of the “carbon tubes” was roughly calculated by 2.3 nm in average according to the 2θ of the $(100')$ reflection.

The hydrothermal process was frequently used in the earlier attempts to achieve a better incorporation of the Mo species into the silica framework [22,23]. However, the Mo loading efficiencies were inferior in the range of <20% in normal cases. The atom geometry of Mo^{VI} did not allow an isomorphic substitution of the silicon atoms [22], so that most of the Mo species were washed off along with the surfactants owing to their weak interplay with the $-\text{Si}-\text{OH}$ groups. Another problem was that the Mo species would react with silica during the thermal treating procedure to form the silicomolybdic acids, refractory to be reduced and carburized [23]. In the present case, however, the “carbon tubes” hindered the blend of the Mo species into the silica walls by posing an isolation belt between them. Thermal treating the $\text{MoC}_x@\text{OMSF}$ sample in O_2 to eliminate the carbon residues did not bring change to the V_{micro} content, indicating the micropores in the sample were contributed by the silica framework rather than the carbon residues. Thus, a direct evidence for the isolating effect of the “carbon tubes” could be found in the V_{micro} contents of the $\text{MoC}_x@\text{OMSF}$ samples, which stabilized at ~10% after the inclusion of MoC_x and regardless of the Mo loading (Table 1). If not, a decrease in the V_{micro} would be observed due to the Mo species penetrating the micropores of the silica framework [24]. The FTIR spectra showed two sets of peaks attributed to the silica matrix (Fig. S3). One at 1080 cm^{-1} with a shoulder peak between 1100 and 1300 cm^{-1} was assigned to the asymmetric stretching of the $\text{Si}-\text{O}-\text{Si}$ bond, while the other one at 811 cm^{-1} was ascribed to the symmetric stretching of the $\text{Si}-\text{O}-\text{Si}$ bond. The two sets of peaks did not undergo any obvious change in

peak intensity after the incorporation of MoC_x , illustrating that the resulting $\text{MoC}_x@\text{OMSF}$ samples preserved the structural integrity of the host silica framework. On the contrary, the peak at 963 cm^{-1} decreased dramatically once MoC_x was included. This peak was attributed to the stretching of the nonbridging oxygen atom in the $\text{Si}-\text{O}-\text{H}$ bond. The shift of this peak to lower wavenumber indicated the change of the degree of the interaction between $-\text{Si}-\text{OH}$ and Mo, with shift to $\sim 950 \text{ cm}^{-1}$ and to $\sim 920 \text{ cm}^{-1}$ corresponding to the formation of $\text{Si}-\text{OH}\cdots\text{Mo}$ and $\text{Si}-\text{O}-\text{Mo}$ respectively [25]. However in this case, no position shift but a dramatic decrease in the peak intensity was observed upon the incorporation of MoC_x . This phenomenon demonstrated the absence of the interplay between the Mo species and the silica framework due to the presence of the “carbon tubes”, while the reduction of the peak intensity implied that the surface $-\text{Si}-\text{OH}$ groups were intimately covered by the graphitic flakes.

The dispersion of the elements within the $\text{MoC}_x@\text{OMSF}$ sample was pictured by EDS elemental mapping, where the maps of Mo and C element matched well with the maps of Si and O element, demonstrating the MoC_x were evenly dispersed throughout the silica framework (Fig. 5f–j). The highly ordered mesostructure was revealed with hexagonal organized domains in TEM images. High-resolution TEM images provided the close-up of the situation inside the silica tubes. No individual particles can be observed probably due to the MoC_x was dispersed in the walls of the “carbon tubes” thus was difficult to be distinguished from the neighboring environment owing to the similar contrast (Fig. 5b–e). The wide-angle X-ray diffraction (WAXRD) patterns exhibited only the background from the silica support irrespective of the Mo loading (Fig. S4). This might be due to the MoC_x species were highly dispersive and in small size below the detection limit of X-ray scattering. To exclude the interference from the silica support, WAXRD pattern of the reference sample free of silica was collected. The resolved three broad peaks at $2\theta = 37.1^\circ$, 62.2° , 74.2° in the diffractogram were indexed to (111) , (220) , and (311) reflections of fcc $\alpha\text{-MoC}_{1-x}$, which could be seen as an evidence for the yield of the carbide phase within the $\text{MoC}_x@\text{OMSF}$ samples. The reason for the formation of $\alpha\text{-MoC}_{1-x}$ rather than $\beta\text{-Mo}_2\text{C}$ in the pyrolysis of the $\text{MoC}_x@\text{OMSF}$ preform was the presence of the P123 micelles. The transformation of metastable α phase carbide into stable β phase carbide was observed with elevated temperature during the pyrolysis of Mo^{VI} –melamine hybrids [14]. However, the metastable α phase MoC_x could be stabilized in a carbon-rich environment [26],

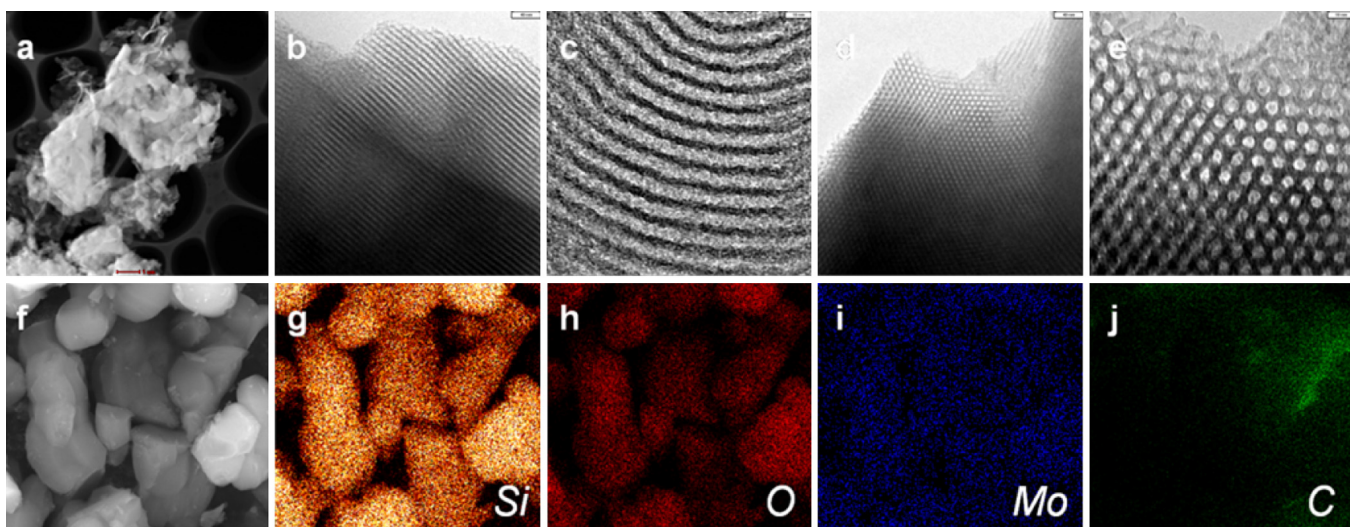


Fig. 5. HAADF-STEM image (a), TEM images (b–e), and EDS elemental mapping (g–j) of the selected area (f) of $\text{MoC}_x@\text{OMSF-6}$.

which in the present case was created by the thermal decomposition of the P123 micelles. The DTA curve of the $\text{MoC}_x@\text{OMSF}$ preform also indicated the transformation of the carbide phase (Fig. S1b). The first endothermic regime starting from RT to $\sim 700^\circ\text{C}$ was due to the thermal decomposition of the P123 micelles within the $\text{MoC}_x@\text{OMSF}$ preform, while the second endothermic regime starting from $\sim 800^\circ\text{C}$ was supposed to result from the transformation of $\alpha\text{-MoC}_{1-x}$ into $\beta\text{-Mo}_2\text{C}$, which process was accompanied by the dissolve out of the lattice carbon and further reduction of the Mo species. The XPS analysis was performed to determine the valence state of the Mo element in the $\text{MoC}_x@\text{OMSF}$ samples. The de-convolution of Mo 3d XPS spectrum gave four peaks ascribed to the most common Mo^{V} and Mo^{VI} oxides (Fig. S5a). The oxidation of the MoC_x species upon exposure to air was proposed to account for the absence of the peak due to the carbodic Mo which was reported to locate between 283 and 284 eV. The oxidation in the present case was much easier to penetrate from the carbide surface to the bulk owing to the relatively smooth inward diffusion of oxygen atoms within the ultra-small MoC_x species [27]. Correspondingly, the de-convolution of the C 1s XPS spectrum did not give peak due to the lattice carbon but three peaks situated at 284.2, 285.0, and 286.8 eV in accordance with sp^2 , sp^3 hybridized, and oxygen-bonded carbon (Fig. S5b).

3.3. Catalytic performance

The hydrogenation of naphthalene was used to evaluate the potential of the $\text{MoC}_x@\text{OMSF}$ composites for catalytic use. The products of this consecutive hydrogenation reaction varied depending on the type of the catalyst. The noble metals, such as Pt, Pd, and Ru, were of choice if the over-hydrogenated product of decalin was desired [28–30]. On the contrary, the catalysts with moderate hydrogenating ability were considered for specific production of tetralin. Molybdenum carbides were classified into the latter type of the catalyst that could perform the naphthalene hydrogenation with ultra-high selectivity to tetralin [8,14]. The hydrogenation performance of the $\text{MoC}_x@\text{OMSF}$ samples was depicted in Table 2. As can be seen, all the samples including the bulk $\beta\text{-Mo}_2\text{C}$ performed the hydrogenation with high selectivity of $>98\%$ to tetralin owing to the moderate hydrogenating ability of molybdenum carbide with respect to noble metals. When conducting the naphthalene hydrogenation over the Mo/OMSF sample, the selectivity to tetralin dropped down to $\sim 75\%$ (Table 2). The phenomenon was explained by the reorganization that the

very strong reactivities of early transition metals can be tamed by the formation of carbide [31], supporting the formation of MoC_x within the $\text{MoC}_x@\text{OMSF}$ samples. The TOF value was observed to undergo an obvious increase from the $\text{MoC}_x@\text{OMSF-70}$ sample to the $\text{MoC}_x@\text{OMSF-50}$ sample. Over the two samples, the pore diameter also underwent an obvious increase. It was supposed that when the pore diameter was smaller than a certain value, the silica tubes were unable to accommodate the reactant flow in whole. Part of the flow directly ran off and increased the content of naphthalene in the products. As the pore diameter increased, the diffusion limitation on the reactant flow diminished. The hydrogenation became reaction control. Therefore, as indicated by the almost identical activities of the $\text{MoC}_x@\text{OMSF-X}$ ($X = 50, 30, 15, 10, 6$) samples, the dispersions of the MoC_x species within these samples appeared to be the same. All the $\text{MoC}_x@\text{OMSF}$ samples exhibited much higher TOF values in comparison to the bulk $\beta\text{-Mo}_2\text{C}$, implying highly dispersive MoC_x species benefited the exposure of the active sites. The stability of the $\text{MoC}_x@\text{OMSF}$ sample was also enhanced with respect to the bulk $\beta\text{-Mo}_2\text{C}$, as the former maintained the conversion of naphthalene above 70% in the first 24 h while the latter presented a lasting deactivation even at the initial stage of the hydrogenation (Fig. 6). The good stability of the $\text{MoC}_x@\text{OMSF}$ sample was due to the incorporation of the MoC_x species into the walls of the “carbon tubes”, which could prevent the MoC_x species from

Table 2
Catalytic performance of the samples in naphthalene hydrogenation.

Sample	Nap. conversion ^a (%)	Selectivity to tetralin (%)	TOF (h^{-1})	Pore diameter (nm)
Pure OMSF ^b	–	–	–	6.1
$\text{MoC}_x@\text{OMSF-70}$	62.7	98.2	523.7	6.9
$\text{MoC}_x@\text{OMSF-50}$	81.4	98.4	679.8	7.3
$\text{MoC}_x@\text{OMSF-30}$	82.3	98.6	687.4	7.3
$\text{MoC}_x@\text{OMSF-15}$	81.2	98.1	678.2	7.3
$\text{MoC}_x@\text{OMSF-10}$	85.9	98.3	717.4	7.5
$\text{MoC}_x@\text{OMSF-6}$	81.3	98.1	679.0	7.5
Bulk $\beta\text{-Mo}_2\text{C}$	1.4	98.5	11.7	–
Mo/OMSF-15 ^c	96.7	75.4	807.6	6.2

^a Conversion of naphthalene.

^b Inert to the hydrogenation.

^c $\text{Si/Mo} = 15$. Reaction conditions: feed rate = 0.05 mL/min (1 wt.% naphthalene in cyclohexane), H_2 flow rate = 50 mL/min, WHSV = 8.7 h^{-1} , $\text{H}_2/\text{oil} = 723$. WHSV was calculated based on the actual weight of Mo. $\text{TOF} = F \times C/M$, where F represented the molar flow rate of naphthalene (mol/h), C was the conversion of naphthalene, while M was the mole of Mo. The catalytic performance represented the state of the catalysts on stream for 12 h.

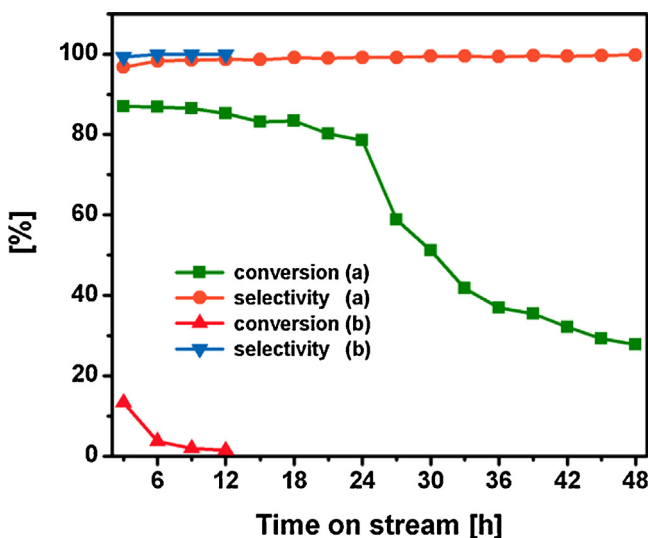


Fig. 6. Long-term catalytic performance of $\text{MoC}_x@\text{OMSF-6}$ (a) and bulk $\beta\text{-Mo}_2\text{C}$ (b) in naphthalene hydrogenation.

agglomeration. The obvious deactivation of the $\text{MoC}_x@\text{OMSF}$ sample after 24 h on stream resulted from the course of the highly active “carbon vacancies” in the MoC_x surface being gradually filled, which was accompanied by the formation of surface carbon deposit and disabled the carbide surface from activating tetralin, leading to increased content of tetralin in the hydrogenation products [8].

4. Conclusions

The full incorporation of MoC_x species into ordered mesoporous silica framework has been realized by using Mo^{VI} –melamine hybrids as the carbide precursors and their interaction with the surfactant micelles. This novel composite possessed a hierarchical structure with *in situ* grew “carbon tubes” attached to the internal surface of the silica framework. MoC_x species were finely dispersed in the walls of the “carbon tubes” and featured good stability in catalytic use, partially overcoming the deactivation issue of the thermal sintering of the carbide particles during catalytic reaction. Yet, some open questions, typical as the inferior Mo loading efficiency, need to be addressed in the future development of this integrated preparation procedure for advanced carbide composites that suit practical catalytic applications.

Acknowledgement

We gratefully acknowledge the financial support provided by the National Natural Science Foundation of China (21373038 and 21428301).

Appendix A. Supplementary data

Supplementary data associated with this article can be found, in the online version, at <http://dx.doi.org/10.1016/j.apcata.2014.11.023>.

References

- [1] R.B. Levy, M. Boudart, *Science* 181 (1973) 547–549.
- [2] M. Pang, C. Li, L. Ding, J. Zhang, D.S. Su, W.Z. Li, C.H. Liang, *Ind. Eng. Chem. Res.* 49 (2010) 4169–4174.
- [3] C.H. Liang, L. Ding, C. Li, D.S. Su, Y.M. Wang, W.Z. Li, *Energy Environ. Sci.* 3 (2010) 1121–1127.
- [4] N.M. Schweitzer, J.A. Schaidle, O.K. Ezekoye, X.Q. Pan, S. Linic, L.T. Thompson, *J. Am. Chem. Soc.* 133 (2011) 2378–2381.
- [5] S.K. Gade, S.J. Chmelka, S. Parks, J.D. Way, C.A. Wolden, *Adv. Mater.* 23 (2011) 3585–3589.
- [6] N. Ji, T. Zhang, M.Y. Zheng, A.Q. Wang, H. Wang, X.D. Wang, J.G. Chen, *Angew. Chem. Int. Ed.* 47 (2008) 8510–8513.
- [7] L. Liao, S.N. Wang, J.J. Xiao, X.J. Bian, Y.H. Zhang, M.D. Scanlon, X.L. Hu, Y. Tang, B.H. Liu, H.H. Girault, *Energy Environ. Sci.* 7 (2014) 387–392.
- [8] M. Pang, C.Y. Liu, W. Xia, M. Muhler, C.H. Liang, *Green Chem.* 14 (2012) 1272–1276.
- [9] R.H. Wang, J. Yang, K.Y. Shi, B. Wang, L. Wang, G.H. Tian, B. Bateer, C.G. Tian, P.K. Shen, H.G. Fu, *RSC Adv.* 3 (2013) 4771–4777.
- [10] S.A.W. Hollak, R.W. Gosselink, D.S. van Es, J.H. Bitter, *ACS Catal.* 3 (2013) 2837–2844.
- [11] J.S. Lee, S.T. Oyama, M. Boudart, *J. Catal.* 106 (1987) 125–133.
- [12] P. Afanasyev, *Inorg. Chem.* 41 (2002), 5317–5319.
- [13] Q.S. Gao, C.X. Zhang, S.H. Xie, W.M. Hua, Y.H. Zhang, N. Ren, H.L. Xu, Y. Tang, *Chem. Mater.* 21 (2009) 5560–5562.
- [14] M. Pang, X.K. Wang, W. Xia, M. Muhler, C.H. Liang, *Ind. Eng. Chem. Res.* 52 (2013) 4564–4571.
- [15] P.Y. Wu, S.F. Ji, L.H. Hu, J.Q. Zhu, C.Y. Li, *J. Porous Mater.* 15 (2008) 181–187.
- [16] C.H. Liang, P.L. Ying, C. Li, *Chem. Mater.* 14 (2002) 3148–3151.
- [17] L.H. Hu, S.F. Ji, Z. Jiang, H.L. Song, P.Y. Wu, Q.Q. Liu, *J. Phys. Chem. C* 111 (2007) 15173–15184.
- [18] H. Wang, A.Q. Wang, X.D. Wang, T. Zhang, *Chem. Commun.* 22 (2008) 2565–2567.
- [19] K.G. Vassilev, D.K. Dimov, R.T. Stamenova, R.S. Boeva, Ch.B. Tsvetanov, *J. Polym. Sci. Part A: Polym. Chem.* 24 (1986) 3541–3554.
- [20] D.Y. Zhao, J.L. Feng, Q.S. Huo, N. Melosh, G.H. Fredrickson, B.F. Chmelka, G.D. Stucky, *Science* 279 (1998) 548–552.
- [21] Y. Wang, B. Zibrowius, C.M. Yang, B. Spliethoff, F. Schüth, *Chem. Commun.* 1 (2004) 46–47.
- [22] J.A. Melero, J. Iglesias, J.M. Arsuaga, J. Sainz-Pardo, P. de Frutos, S. Blazquez, *Appl. Catal. A: Gen.* 331 (2007) 84–94.
- [23] P.C. Bakala, E. Briot, L. Salles, J.M. Brégeault, *Appl. Catal. A: Gen.* 300 (2006) 91–99.
- [24] S. Silva, A. Chaumonnot, A. Bonduelle-Skrzypczak, F. Lefebvre, S. Loridan, V. Dufaud, *ChemCatChem* 6 (2014) 464–467.
- [25] M.S. Morey, J.D. Bryan, S. Schwarz, G.D. Stucky, *Chem. Mater.* 12 (2000) 3435–3444.
- [26] H. Preiss, B. Meyer, C. Olschewski, *J. Mater. Sci.* 33 (1998) 713–722.
- [27] K.J. Leary, J.N. Michaels, A.M. Stacy, *J. Catal.* 101 (1986) 301–313.
- [28] S. Albertazzi, G. Busca, E. Finocchio, R. Glöckler, A. Vaccari, *J. Catal.* 223 (2004) 372–381.
- [29] K. Ito, Y. Kogasaka, H. Kurokawa, M. Ohshima, K. Sugiyama, H. Miura, *Fuel Process. Technol.* 79 (2002) 77–80.
- [30] S.D. Lin, C.S. Song, *Catal. Today* 31 (1996) 93–104.
- [31] J.G. Chen, *Chem. Rev.* 96 (1996) 1477–1498.